 https://doi.org/10.3311/PPch.22213

Periodica Polytechnica Chemical Engineering, 67(3), pp. 396–406, 2023

Study on Corrosion Characteristics of Aluminum Alloy Al3102 in Sulfate-reducing Bacteria Environment and Investigating the Use of *Azadirachta indica* Leaves Extract in its Control

Noyel Victoria Selvam[1], Akansha Sharma[1], Manivannan Ramachandran[1*]

[1] Department of Chemical Engineering, National Institute of Technology, Raipur, G.E. Road, 492010 Raipur, Chhattisgarh, India
[*] Corresponding author, e-mail: rmani.che@nitrr.ac.in

Received: 16 March 2023, Accepted: 15 June 2023, Published online: 10 July 2023

Abstract

An effort to understand the corrosion characteristics of aluminium Al3102 alloy in a neutral medium in the presence of *Desulfovibrio desulfuricans* was made. The corrosion rate increased up to tenfold in the bacterial medium in comparison to the control (abiotic) medium. Scanning electron microscopy (SEM) studies showed substantial sulfate-reducing bacteria (SRB) adhesion on the alloy surface and pit formation. Supplementation of 1000 ppm *Azadirachta indica* leaves extract decreased corrosion by 82%. Sulfide analysis, SEM, and X-ray photoelectron spectroscopy (XPS) studies showed a significant effect of neem leaf extract (NLE) on bacterial metabolic activity and confirmed the adsorption of the inhibitor molecules on Al3102 surface. Electrochemical impedance spectroscopy studies showed that the NLE formed a highly resistive external layer which protected the alloy surface from the corrosive effects. The gas chromatography-mass spectroscopy studies (GC-MS) showed appreciable amount of esters, terpenoids, heterocyclic nitrogen, sulfur compounds, and organic bromine compounds in NLE.

Keywords

Al3102, *Desulfovibrio desulfuricans*, neem leaf, corrosion, XPS, GC-MS

1 Introduction

Damage to the metal structures by the activity of microorganisms has been an issue of concern for many decades. The activity of microorganisms and the subsequent damage to the metal structures has been termed microbially influenced corrosion (MIC). Unlike corrosion caused by corrosive chemical activity, the occurrence of MIC is widespread ranging from simple wastewater-carrying lines, wastewater treatment plants, cooling towers, and heat exchangers to sophisticated nuclear reactor coolant systems, parts, and machinery of ships and aircraft. The damages caused by the MIC sometimes cause serious consequences such as loss of lives [1]. Microbe-induced corrosion is always the consequence of the activity of various types of microbes. Biofilm on the metal surface houses various types of bacteria with an aerobic population occupying the top layer where oxygen is available in plenty. At the inner zones of the biofilm which is closer to the metal surface and where oxygen is scarce, the anaerobic population predominates. Though the MIC is a contribution of different types of bacterial strains, a significant portion of the damage is contributed by the activity of the anaerobic bacterial population most importantly, sulfate-reducers. The sulfate-reducing bacteria (SRB) are known to attack metals and concrete structures. SRB participates in the electron transfer processes of the metal system and produces the respective metal sulfides. These metal sulfides have been identified as corrosion promoters due to the formation of local concentration cells [2].

Aluminum is one of the industrially preferred metals due to its excellent corrosion-resistant properties. Aluminum and its alloys are used in the manufacture of cooking vessels, storage containers, condenser tubes, fins, and as construction material in marine and aviation industries. In contact with air, Al forms a corrosion-resistant oxide film on the surface. However, the native film has been found to be less resistant to corrosion under adverse conditions. The response of Al and its alloys varies with respect to the medium in which they are present. In fact, the composition of the alloys and the nature of the medium in which the SRB and the metal are present play a major

Cite this article as: Selvam, N. V., Sharma, A., Ramachandran, M. "Study on Corrosion Characteristics of Aluminum Alloy Al3102 in Sulfate-reducing Bacteria Environment and Investigating the Use of *Azadirachta indica* Leaves Extract in its Control", Periodica Polytechnica Chemical Engineering, 67(3), pp. 396–406, 2023. https://doi.org/10.3311/PPch.22213

role in dictating corrosion characteristics. In the saline medium, SRB was found to protect Al 5052 from the corrosive effects of the halide ions [3]. However, studies on Al 5052 in Postgate C medium containing SRB reported severe pitting corrosion [4]. In another study with Al 5052 and Al alloy containing zinc, cadmium, and indium, in Postgate C medium containing SRB, the Al-Zn-Cd-In alloy presented more corrosion damage due to the SRB activity when compared to Al 5052 which showed relatively less pitting [5]. It was suggested that the addition of other elements to Al during alloy formation helps in enhancing the SRB electron transfer activity by breaking the passive layer [5]. It was also reported that though the role of Al in the electron transfer activity of SRB is not dominant as in the case of iron, it does contribute to a little extent leading to metal dissolution. The corrosion products were found to consist of $Al(OH)_3$, Al_2O_3, and Al_2S_3 [5]. With limited reports available on SRB interaction with Al and its alloys, investigation of the same has become important considering the widespread applications of Al and its alloys. There are very limited reports on the control of SRB-caused corrosion damage in Al and its alloys [6, 7]. Porous self-assembled monolayers of 1H,1H,2H,2H-perfluorodecyltriethoxysilane were formed on anodized Al (99.9 % pure) into which lubricant perfluoropolyether was filled. Studies over a seven-day period in SRB containing Postgate medium showed that the coating prevented the SRB adhesion leading to increased corrosion resistance [7]. Similarly, Al (>99.99%) coated with antimicrobial agents triclosan and cetyl trimethyl ammonium bromide containing tannin-FeIII complex effectively decreased SRB adhesion up to 14 days [6]. Lam et al. reported that the amino acids, such as d-methionine, d-leucine, d-tyrosine and d-phenylalanine, have the tendency to control the biofilm formation and reduce the biocorrosion [8]. Reports on the use of an environmentally friendly corrosion inhibitor /biocide to control the SRB-caused damages on Al and its alloys are still lacking. Neem leaves extract was found to be effective in control of microbial corrosion of copper caused by *Arthrobacter sulfureus* [9]. The present study involves understanding the corrosion characteristics of aluminum alloy Al3102 alloy in a modified Baar's medium. In addition, the work also investigates the efficacy of *Azadirachta indica*, the Indian neem leaves extract (NLE) in the control of SRB-induced corrosion. *Desulfovibrio desulfuricans* (*DD*) belong to SRB group and has been used in this work.

2 Experimental

2.1 Medium and *D. desulfuricans* strain

Analytical-grade chemicals from Loba Chemie (India) were used in the study. The nutrient medium used for the study was modified Baar's medium consisting of calcium and magnesium sulfates as the sulfate source, ammonium chloride, di-potassium hydrogen phosphate as the phosphate nutrient source, sodium lactate as the carbon provider, and ferrous ammonium sulfate as the iron source, the composition of which is mentioned elsewhere [10]. The SRB strain, *Desulfovibrio desulfuricans* was purchased from NCIM, Pune, India.

2.2 Al specimen preparation

Aluminum 3102 sheets (Al3102) of 1 mm thickness were purchased from the local market and were used for corrosion studies. The Al3102 sheet was made into small coupons (1 cm × 1 cm), polished with grit paper from coarse to fine grade. After polishing, the coupons were cleaned in acetone and deionized water, dried, and stored in an airlock container. For both the weight loss and electrochemical experiments, the sides and one face of the coupons were properly sealed using sticky Teflon tape. It was made sure that only one surface of the sample is in contact with the corrosive medium and that the available area is 1 cm^2. For the weight loss studies, a polymeric thread was fixed to the sealed side of the coupons to keep them hanging in the corrosive environment. For the electrochemical trials, a copper wire was connected to the unexposed surface before sealing it with Teflon tape.

2.3 Inhibitor preparation

Neem leaves were powdered after proper cleaning and drying. The powder was soaked overnight in methanol and the filtrate was subjected to 5 h reflux at 50 °C [11]. The neem leaf extract (NLE) was collected after vacuum evaporation of the solvent. The concentration of the NLE used for the studies was 1000 ppm.

2.4 Weight loss and electrochemical investigations

Both the weight loss and electrochemical investigations were conducted for four weeks. The details of the nutrient medium used for the studies and their notations are shown in Table 1.

For monitoring the weight loss of the Al3102 sample in different media, pre-weighed samples were kept hanging inside the test tubes containing different media and incubated at 37 °C in dark. All the samples and the medium were

Table 1 Details of the nutrient medium used in the study

Notation used	Composition
MC	Baar's medium
MCI	Baar's medium + NLE
MB	Baar's medium + *DD*
MBI	Baar's medium + *DD*+ NLE

properly sterilized and bubbled with nitrogen to ensure anaerobic conditions. Four samples were taken out every week, washed to remove the external films formed [12], and dried and weight loss was noted. The weight loss values were utilized for the calculation of the corrosion rates (C_R) and efficiency of corrosion inhibition (η). The C_R was calculated using the standard method reported elsewhere [9]. The efficiency of the NLE in controlling the *DD*/chemical-induced corrosion in Al3102 samples is estimated by comparing weight loss observed in uninhibited (MB / MC) and inhibited (MBI / MCI) samples using the standard formula reported in our earlier report [9].

For the electrochemical investigations, along with the prepared Al working electrodes, platinum counter and Ag/AgCl reference were used. The electrochemical investigations were performed using a CH6091E electrochemical analyzer (CH instruments, USA). For the electrochemical runs, the corresponding nutrient medium at 37 °C was the electrolyte. The potentiodynamic polarization (PDP) studies were made in the voltage range ± 250 mV from the open circuit potential (OCP) at a step rate of 1 mV s^{-1}. The electrochemical impedance spectroscopy (EIS) was performed between 10^5 and 0.1 Hz with a sine wave of rms amplitude 10 mV. Prior to each electrochemical run, the system was maintained at the open circuit potential for 30 min. Tafel extrapolation calculations from the PDP runs were performed by employing the CH-electrochemical analyzer software to find out the corrosion current (I_c) and potential (E_c). The data from EIS study were validated using Kramers Kronig Transformation (KKT) and the appropriate electrical circuit for the system was obtained using ZSimpWin software [13].

3 Results and discussion

3.1 Weight loss studies

The results of the weight loss studies for Al3102 in different media for every week are shown in Fig. 1 (a) and (b). The extent of Al3102 corrosion in the MC and MCI media has been observed to be very less. In the MC media, the C_R for the first two weeks was almost the same 0.013 mmpy which decreased to 0.001 mmpy in the fourth week. This trend can be attributed to the deposits of corrosion reaction products with prolonged immersion that helps to suppress corrosion. With the addition of NLE, the corrosion was found to be completely stopped in the MCI (abiotic) media.

In the presence of *Desulfovibrio desulfuricans*, the C_R increased to 0.05 mmpy which is 3.8 times higher than that of the first week C_R observed with MC medium. The C_R decreased slightly till the third week and remained stable thereafter. The biofilm produced by bacterial metabolism prevents the passage of the corrosive entities from reaching the Al3102 surface thus minimizing the C_R. With the addition of the NLE, the C_R decreased to 0.01 mmpy during week 1 and further dropped to 0.004 mmpy in week 4. Thus, the NLE plays the role of an antibacterial agent which controls the activity of the *DD* and helps in minimizing the C_R. A zero C_R value observed for the samples immersed in the MCI medium shows that apart from the antibacterial action, the NLE also functions as corrosion inhibitor by adsorption on the metal surface. On an average, the corrosion decreased by 82% for the Al3102 samples immersed in *DD*-containing media. Fig. 1 (c) shows the dissolved sulfide concentration at different immersion periods in MB and MBI samples. It can be seen that the NLE significantly lowers the sulfide concentration which shows that it influences the metabolic process of the *DD*.

3.2 Morphological studies

The surface images from SEM analysis for the Al3102 coupons in MB and MBI medium at different immersion periods are given in Figs. 2 and 3. Fig. 2 (a) and (b) show the SEM results for the Al3102 coupons with an external film formed on it, after one week immersion period in MB and MBI medium, respectively. In the MB sample,

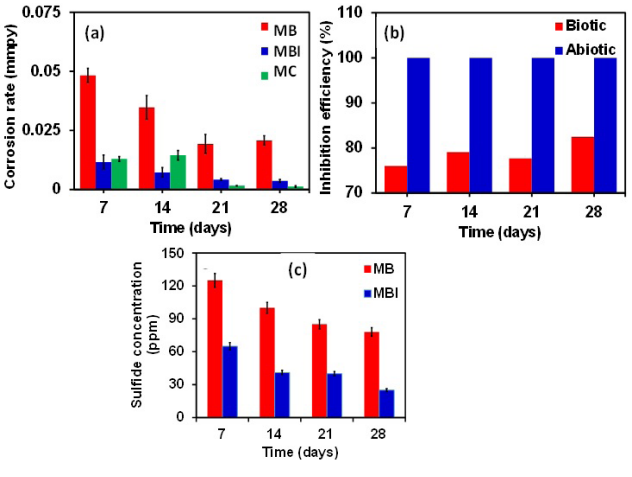

Fig. 1 Effect of immersion time on (a) corrosion rate (b) inhibition efficiency and (c) sulfide concentration

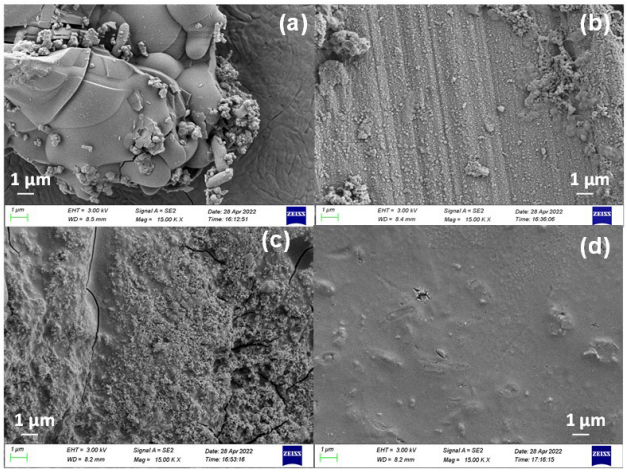

Fig. 2 SEM images of Al3102 coupons after one week immersion period in (a) MB and (b) MBI medium with the external film (c) MB and (d) MBI medium after removing the external film

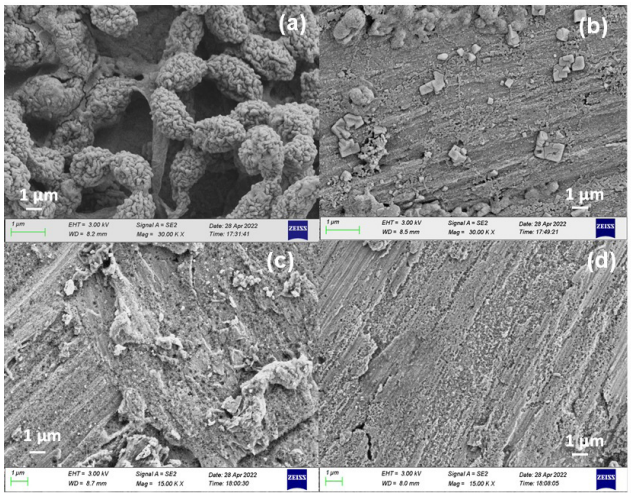

Fig. 3 SEM images of Al3102 coupons after three weeks immersion period in (a) MB and (b) MBI medium with the external film (c) MB and (d) MBI medium after removing the external film

large globular structures can be observed with more rod-shaped bacteria. The globular features are not continuous; however, the entire sample surface is covered with a continuous filamentous network. The sample in MBI media does not show any significant biofilm formation and the bacterial attachment observed on the surface is less. In a few places, tiny globular mesh-like patterns are visible. However, the external layer formed is not dense and continuous since the polishing grooves are visible. Fig. 2 (c) and (d) show the images of Al3102 coupons after one week immersion period in MB and MBI samples after removing the external film formed on them. The MB sample shows the features of pitting. Fig. 3 (a) and (b) show the surface images of the Al3102 coupons immersed in the MB and MBI media after three weeks of immersion without removing the external layer formed. The Al3102 coupon which was in contact with MB media presents the existence of two different kinds of layers. The nature of these layers differs significantly from that observed from the Al3102 coupons in contact with MB media after one week immersion period. The MB sample after three weeks shows well-developed regularly repeating globular structures and an inner continuous thin layer. Such well-developed features suggest the existence of an active bacterial population. On the other hand, the MBI sample presents similar features to that of the first week MBI sample. Fig. 3 (c) and (d) show the images of Al3102 coupons in MB and MBI medium without film after three weeks immersion period. The uninhibited sample presents the formation of many larger pits whereas the inhibited coupon shows lower pit propagation.

Table 2 shows the elemental analysis of the Al3102 samples after the first and third-weeks immersion in MB and MBI media. Increased oxygen content in the MBI sample immersed for one week period could be due to the adsorbed inhibitor molecules. Similarly, the third week MBI sample shows increased bromine content which could be due to the adsorption of molecules from the NLE extract.

3.3 Electrochemical tests

3.3.1 Potentiodynamic polarization (PDP)

Fig. 4 (a) and (b) present the PDP plots for Al3102 samples in MB and MBI media respectively at various immersion periods. It is noticed from Fig. 4 (b), that the addition of NLE does not change the shape of the potentiodynamic polarization plots. This shows that the mechanism is not

Table 2 Elements of the external films formed on the Al3102 samples in MB and MBI media at the end of the first and third weeks of immersion

Elements	Atomic %			
	Week 1		Week 3	
	MB	MBI	MB	MBI
O	15.4	28.7	31.2	–
Na	–	–	2.4	2.8
Mg	–	–	1.6	–
Al	84.0	70.8	59.7	79.5
Si	–	–	2.2	2.9
S	0.1	0.1	0.6	0.5
Cl	–	–	0.4	–
Ca	–	–	0.8	–
Fe	–	–	0.5	0.8
Au	0.5	0.4	0.5	0.7
Br	–	–	–	12.7

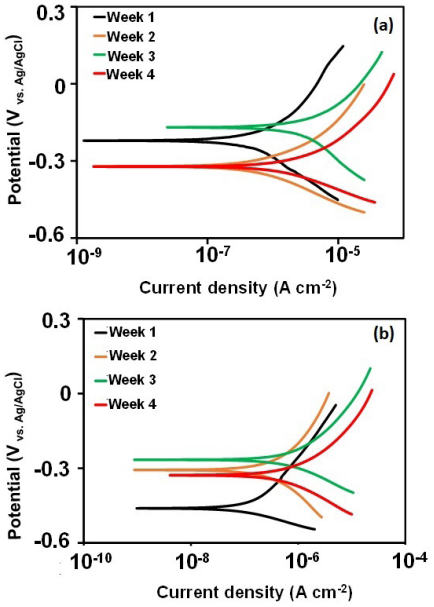

Fig. 4 Potentiodynamic polarization plots for Al3102 in (a) MB and (b) MBI medium at different immersion periods

significantly altered with the addition of the NLE. In the MB samples, the anodic branches move towards the right with an increasing immersion period indicating a surge in the corrosion process with the immersion period. With NLE, both the anodic and cathodic current densities decrease indicating a drop in the respective reaction rates. The E_c values of the MB sample show a negative shift from −230 mV to −320 mV in the second week which shows an increased corrosion rate and matches well with the behavior of the weight loss experiment results. For the third week, it moves in the positive direction and decreases again in the fourth week. Such a fluctuating behavior of E_c can be attributed to the variations occurring in the depth and composition of the external film. In the MBI samples, the E_c values show a positive shift till the third week and show a negative shift in the fourth week. This trend could also be due to the fluctuations in the vicinity, changes in the charge of the biofilm, and its thickness. The non-monotonic trend observed in the E_c values with the immersion period shows that *D. desulfuricans* plays a major role in the electrochemical processes [14].

The I_c values attained by extending the Tafel part of the cathodic and anodic branches are shown in Table 3 along with other Tafel parameters. The I_c values of the MB samples increase continuously till the third week and decrease slightly for the fourth week. A maximum I_c value of 3.1 μA cm^{-2} is observed for the third week. On the other hand, the I_c values for all four weeks in MBI samples are less when compared to the I_c values of the MB samples.

Table 3 Tafel fit parameters for Al3102 in MB and MBI medium at different immersion periods and the inhibition efficiency (IE)

Duration (weeks)	I_c (μA cm^{-2})		E_c (mV)		IE (%)
	MB	MBI	MB	MBI	
	Biotic				
1	0.6	0.1	−230	−462	83.3
2	0.9	0.2	−320	−307	77.7
3	3.1	0.5	−169	−266	83.8
4	1.5	0.4	−322	−328	73.3
	Abiotic				
	MC	MCI	MC	MCI	
1	0.31	0.1	−386	−292	67.7
2	0.35	0.02	−305	−655	94.3
3	0.11	0.005	−231	−297	95.5
4	0.7	0.01	−231	−182	98.5

The I_c values of the MBI samples do not show significant variation with the immersion period. A significant drop in the I_c values with NLE shows that it is effective against *DD*-influenced corrosion of Al in the neutral pH. Fig. 5 shows the PDP plots for the MC and MCI samples. It is obvious that the I_c values observed in the MCI samples are much less when compared to the MC samples indicating that the NLE works as a corrosion resistor against the corrosive action of the medium.

3.3.2 Electrochemical impedance spectroscopy (EIS)

Fig. 6 (a) and (b) show the modulus of impedance (|Z|) variation with frequency for Al3102 coupons in MB and MBI media respectively at different immersion periods. The phase angle (φ) variations are shown in Fig. 6 (c) and (d). The reliability, linearity, and causality of the EIS data are performed by conducting the KKT analysis [9]. In Fig. 6 ((a)–(d)), the symbols represent the values obtained in the experiment, and the continuous lines refer to the KKT simulation results. The experimental and the KKT fit data match well indicating the data set is from a causal, linear, and stable system.

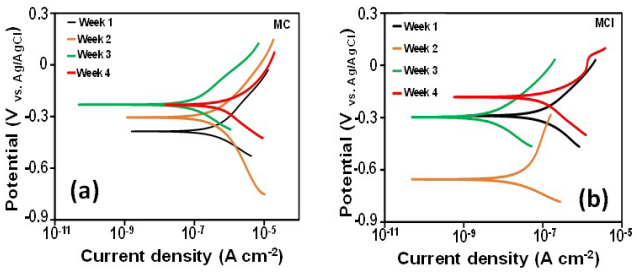

Fig. 5 Potentiodynamic polarization plots for Al3102 at different immersion periods; (a) MC medium; (b) MCI medium

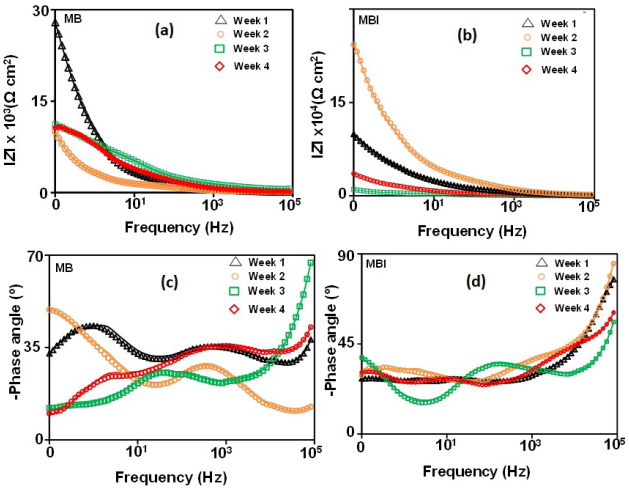

Fig. 6 Bode impedance modulus plot for Al3102 in (a) MB and (b) MBI medium at different immersion periods. Bode phase angle plot for Al3102 in (c) MB and (d) MBI medium at different immersion periods

In Fig. 6 (a), the |Z| remains stable in the high-frequency (HF) zone from 10^5 to 10^3 Hz. It increases gradually for the subsequent frequencies. In the mid to low-frequency (LF) region, a change of slope is observed for the immersion periods 2, 3, and 4 weeks, which are characteristic of pitting corrosion [15]. The slope change observed shifts towards the LF region with respect to the immersion period. The LF region's |Z| for the first week was 27900 Ω cm^2, which significantly decreases to 10000 Ω cm^2 for the subsequent weeks. These observations reveal that significant damage is caused to the material in the presence of *DD*. Evidence of pitting corrosion has also been observed [15].

For the MBI medium in Fig. 6 (b), the |Z| in the LF region significantly increases for the samples with NLE inhibitor. The slope change observed in the middle-frequency (MF) and the LF regions in the case of MB samples, is not observed in the MBI sample. However, |Z| in the LF zone for the third week shows a value closer to 10000 Ω cm^2 which could be due to the changing thickness of the protective films. The value increases again for the fourth week indicating an improvement in the corrosion protection effect.

In Fig. 6 (c), shows the φ variation in MB medium, and the plots show the presence of two-time constants, one extending from HF to MF and the other in the LF region. These are attributed to the corrosion activity and double-layer capacitance [16]. The φ peak in the MF region is broader during the first week indicating the biofilm or external layer formed is well adsorbed on the metal surface [16]. The MF region's φ decreases during the second week and its width decreases. A slight shift towards the LF region is also observed. For the subsequent weeks also the peak in the MF region shifts to the LF side which indicates the progress of corrosion and damages caused by the external film [17]. Moreover, the peaks in the LF region for the third and fourth weeks move towards very low values and the |Z| plot for the same period (MB samples) shows a change in slope. Such a feature of decreased |Z| with a change in slope combined with a very low φ in the LF region corresponds to pitting corrosion [15].

Fig. 6 (d) shows the φ variations in the MBI sample present peaks spreading over wide frequency ranges indicating adsorption of the NLE inhibitor molecules [18]. The φ curve during the first week shows a maximum phase angle value of 77° at the highest frequency and shows a broader MF peak indicating good adsorption of the NLE molecules. The φ at the highest frequency presents a maximum value of 85° for the second week which shows that the maximum thickness of the film is attained in the second week [19]. For the subsequent weeks, the HF region φ drops which indicate the degradation of the protective film and a drop in the corrosion protection effect.

Fig. 7 (a) and (b) show the Nyquist plots of Al3102 samples in MB and MBI media respectively at different immersion periods. In both cases, two depressed semi-circular patterns, which are difficult to distinguish, appear along with the diffusion barrier. The semi-circle pattern present in the HF region is usually ascribed to the external film formation and the LF capacitive trend occurs due to the electron transfer reactions at the metal and the electrolyte interface [20]. With MB sample, the two semi-circular patterns can be easily identified for the third and fourth weeks. The depressed semi-circular pattern is associated with the constant phase element (CPE), a non-ideal form of the capacitor [9]. The diameter of the semi-circle decreases with immersion time owing to the constantly changing biofilm depth profile, ionic concentration, and the products of corrosion reactions on the metal surface. A progressive drop in the impedance values with immersion time shows the progress of corrosion.

The Nyquist plot of MBI samples shows a significant increase in the impedance values. The plot shows two depressed semi-circles one in the HF region and the other in the LF zone. The presence of Warburg diffusion resistance is also obvious in the Nyquist plots. The diameter of the semi-circle increases till the second week and then drops for the third week. This again increases during the fourth week. This fluctuating trend is the result of the changes observed in external films as already mentioned. Thus, the NLE serves to protect the corrosion of the Al sample till the second week, and its effect drops for the subsequent weeks.

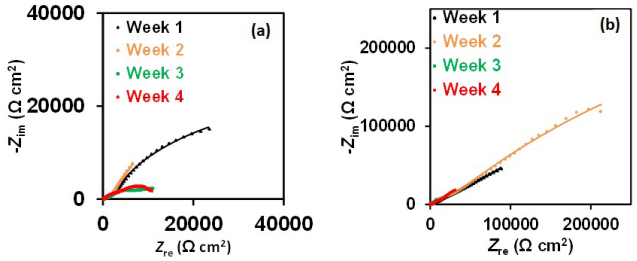

Fig. 7 Nyquist plot for Al3102 coupon in (a) MB and (b) MBI medium at different immersion periods

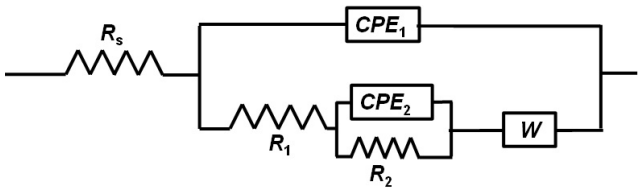

Fig. 8 The electrical circuit used to model the Al3102 system

Fig. 8 shows the electrical equivalent circuit (EEC) which is used to model the EIS observations. Two-time constants with Warburg diffusion element have been identified from the Bode plots and hence an EEC with two CPE and a Warburg element (W) as shown in Fig. 8 has been used. The CPE has been considered in EEC due to the appearance of a depressed semicircle in the Nyquist plots of all the samples. The Warburg impedance can be represented using Eq. (1) [21]:

$$Z_w = \sigma\omega^{-0.5}(1-j). \quad (1)$$

In Eq. (1), σ is the Warburg coefficient ($\Omega\ cm^2\ s^{-0.5}$) and the angular frequency ω (rad s^{-1}) is given by 2 πf. Table 4 shows the best-fit parameters of MB and MBI systems corresponding to the EEC. The Warburg coefficient (σ) helps in measuring the resistance of the external porous films. A higher value of σ shows higher resistance to the flow of corrosive medium through the film. In Table 4, the values of σ are higher for the MBI samples indicating higher diffusion resistance to the flow of the corrosive medium [21].

The total resistance for the MBI system is high for all the immersion periods. The capacitance values keep on changing with the immersion period in both cases due to the constantly varying thickness, composition, and conducting nature of the layers formed on the metal surface.

3.4 XPS investigations

Fig. 9 gives the full spectrum view of XPS analysis of the Al3102 samples immersed in MB and MBI samples after three weeks immersion period with the film formed on them. The MB coupon shows the presence of the sulfide group whereas, the MBI sample does not show the presence of sulfide. The presence of the O1s group is identified from the peaks around 530 eV. The peak at 531.8 eV in MB

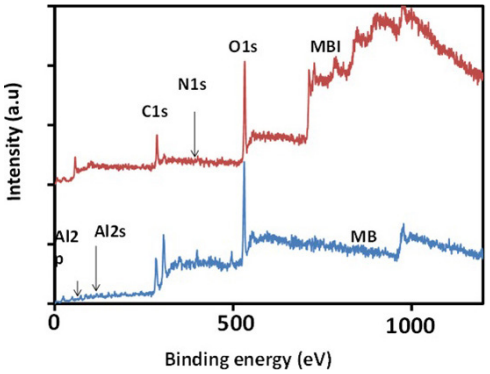

Fig. 9 Wide range XPS spectra for Al3102 coupons immersed in MB and MBI media after three weeks of immersion periods with an external film formed on it

Table 4 EEC fit parameters for Al3102 system in MB and MBI media at different immersion periods

Parameters	MB				MBI			
	1	2	3	4	1	2	3	4
R_s ($\Omega\ cm^2$)	74	211	300	97	188	200	147	300
$CPE_1 - Y_1$ ($\mu S\ s^n\ cm^{-2}$)	29.5	15.5	0.01	16.8	0.02	0.4	14.6	0.03
$CPE_1 - n_1$	0.5	0.6	1.0	0.5	0.9	0.6	0.6	1.0
C_1 ($\mu F\ cm^{-2}$)	5.6	1.4	0.01	1.9	0.004	0.02	1.9	0.02
R_1 ($\Omega\ cm^2$)	8232	1296	609	6931	2910	28400	5071	1047
$CPE_2 - Y_2$ ($\mu S\ s^n\ cm^{-2}$)	7	101	19	20	8	4	104	21
$CPE_2 - n_2$	0.9	0.7	0.5	0.9	0.4	0.5	1.0	0.4
R_2 ($\Omega\ cm^2$)	77050	7319	9769	4981	189100	924800	2698	37330
C_2 ($\mu F\ cm^{-2}$)	6.4	86.1	3.4	16.8	17.7	18.7	104.3	15.4
W ($S\ s^{0.5}\ cm^{-2}$)	2.5	0.3	4.9	16.3	0.1	0.2	1.2	0.2
R_{total} ($\Omega\ cm^2$)	85282	8615	10378	11912	192010	953200	7769	38377
σ ($\Omega\ cm^2\ s^{-0.5}$)	0.4	2.9	0.2	0.1	10.1	4.7	0.8	4.4

sample corresponds to ketones [22]. *Desulfovibrio desulfuricans* is known to produce certain forms of ketones during its metabolic activity [23]. The presence of a peak at 532.8 eV in the case of the MBI sample shows the presence of hydroxyl and epoxy functional groups [24]. Table 5 shows the atomic percentage of the elements in MB and MBI samples in XPS analysis. The absence of sulfur in the MBI sample shows that the NLE has minimized the *Desulfovibrio desulfuricans* metabolic activity. The Al2p and Al2s de-convoluted spectra for the Al samples in MB and MBI media are shown in Fig. 10 (a)–(d). The Al2p spectrum of the MB sample (Fig. 10 (a)) shows the presence of Al_2S_3 (74.3 eV) and Al_2O_3 (74.7 eV) [25]. The sulfide ions formed due to the sulfate reduction step react with the Al^{3+} to produce Al_2S_3 [5]. The Al2p spectrum of the MBI sample (Fig. 10 (b)) shows the presence of oxides and hydroxides of aluminum formed by the reaction of the metal ions with the environment. It also shows the presence of Al-N group which could be due to the adsorption

Table 5 The atomic concentration of the elements from XPS analysis

Element	Atomic %	
	MB	MBI
C1s	48.92	43.53
N1s	0	1.92
O1s	45.08	46.79
Na1s	1.75	0.59
Mg2s	0	3.29
Al2p	0	1.86
Al2s	0.37	1.33
S2p	1.09	
Ca2p	2.8	0.68

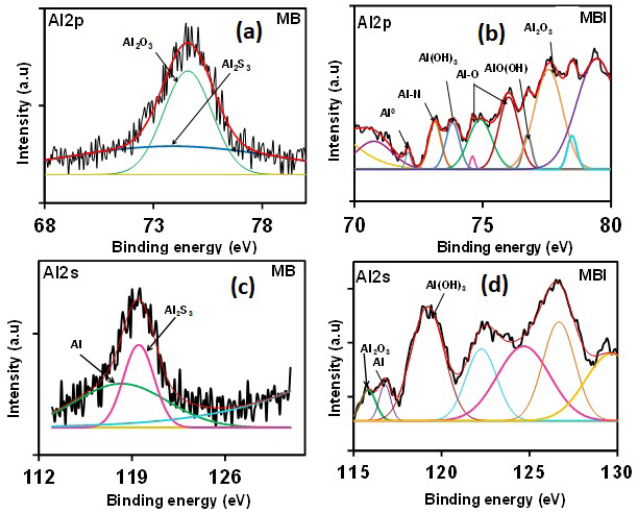

Fig. 10 Deconvoluted Al2p spectra of Al3102 samples in (a) MB and (b) MBI media after three weeks of immersion. Al2s spectra for Al samples in (c) MB and (d) MBI media after three weeks of immersion

of nitrogen-containing groups from NLE. The Al2s spectrum for the MB sample (Fig. 10 (c)) confirms the presence of Al_2S_3 [26]. Further, the Al2p spectrum of the MB sample (Fig. 10 (a)) also shows the presence of Al_2S_3. The peaks at 123.6 eV and 126 eV in the Al2s plot of the MBI sample (Fig. 10 (d)) could be due to the adsorbed halogen-containing compounds from NLE [27]. The C1s spectra for the MB samples (Fig. 11 (a)) show a peak at 284.8 eV related to the C-C group which was observed in many studies related to *DD* biofilm and has been attributed to the presence of amino acids [28, 29]. The carbon spectra for the MBI sample (Fig. 11 (b)) show a prominent signal at 288.9 eV due to the carboxylic or ester groups. This confirms the adhered NLE molecules on the Al surface. O1s spectra of MB sample (Fig. 11 (c)) shows a peak at 532 eV corresponding to the C-O groups of the biofilm [30]. The deconvoluted O1s (Fig. 11 (d)) spectra for the MBI sample show the presence of esters (533.3 eV) and C-OH (534.7 eV) groups adsorbed onto the Al3102 surface [31]. The N1s spectra for the MB sample (Fig. 12) show peaks at 398.5 eV and 400 eV which confirms the metal-N bonds (N-Me) and C-N/C-N-O groups individually, and these findings match well with the

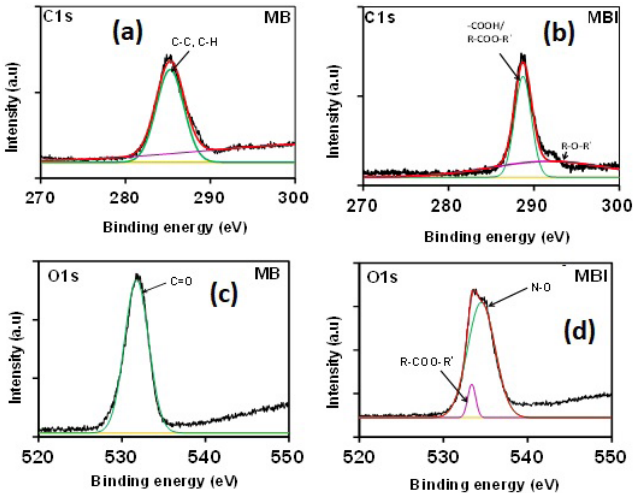

Fig. 11 Deconvoluted C1s plot of Al3102 samples in (a) MB and (b) MBI media after three weeks of immersion. O1s spectra for Al samples in (c) MB and (d) MBI media after three weeks of immersion

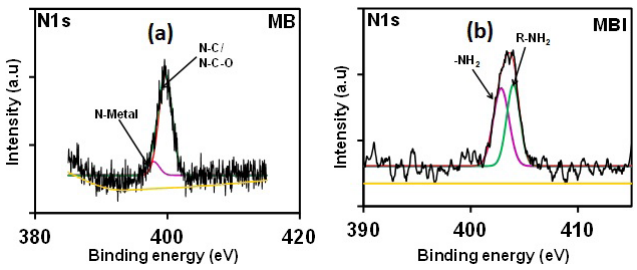

Fig. 12 Deconvoluted N1s plot of Al3102 samples after three weeks of immersion; (a) MB medium; (b) MBI medium

earlier reports by other groups. These peaks are a contribution from the bio-polymeric substances of the biofilm [32]. In addition, N1s peaks at 402.8 eV and 403.9 eV present in the MBI sample (Fig. 12) are due to the adsorbed nitrogen-containing NLE molecules [32].

3.5 GC-MS studies of NLE

The results from the GC-MS investigation of NLE are presented in Table 6 and it shows the presence of significant quantities of esters, heterocyclic sulfur compounds, ketones, and terpenoids. The O1s and the C1s plots for the MBI sample show the existence of adsorbed ester compounds. Table 6 for NLE shows the presence of various steroid esters at 38 min, 50.25 min, and 53.08 min. These three esters constitute about 46.74% of NLE. The Al2s spectra and the EDX analysis of the third-week MBI sample show the presence of bromine which could have come from the heterocyclic nitrogen compound – acridinedion derivative which comes out at 43.42 min. The attachment of these functional groups on Al3102 surface helps to protect it against corrosion. Apart from these, these compounds are also known for their antibacterial activity [33] which helps in the control of the *DD* population.

3.6 Mechanism

Fig. 13 shows the mechanism of corrosion caused by *DD* in the Al3102 sample with and without NLE. Results from different studies have shown that supplementation of 1000 ppm NLE has protected the aluminum metal from the corrosive effects of *D. desulfuricans* to a significant extent. From the studies, the extract offers better corrosion control for two weeks, after which the effect slightly decreased. The XPS analysis confirms the presence of an external layer comprising of aluminum oxide, hydroxides, and sulfides on the MB specimen. Whilst the MBI specimen shows no sulfide which affirms the NLE effect of *DD*. The presence of esters, amines, and other organic groups along with Al_2O_3 is observed in MBI specimen. Based on the above results the following mechanism shown in Fig. 13 (MB) can be proposed [4, 5].

The corrosive environment leads to the generation of aluminum ions by anodic dissolution given by Eq. (2) [4, 5]:

$$Al \rightarrow Al^{3+} + 3e^{-}. \tag{2}$$

Water dissociation gives rise to the formation of H^+ and OH^- radicals (Eq. (3)) which further take part in the reactions:

$$H_2O \rightarrow H^+ + OH^-. \tag{3}$$

The H^+ ions move towards the cathode and take part in the hydrogen generation reaction given by Eq. (4) [4, 5]:

$$H^+ + e^- \rightarrow [H], \tag{4}$$

The hydrogen uptake facilitates electron transfer and reduction of SO_4^{2-} to sulfide by the *DD* given by Eq. (5):

$$SO_4^{2-} + 8[H] + H^+ \rightarrow HS^- + 4H_2O. \tag{5}$$

The produced HS^- undergoes a reversible reaction which results in the production of H_2S (Eqs. (6) and (7)) [34]:

$$HS^- \leftrightarrow H^+ + S^{2-}, \tag{6}$$

$$HS^- + H^+ \leftrightarrow H_2S. \tag{7}$$

The HS^- ion further reacts with Al^{3+} ions which gives rise to the formation of Al_2S_3 (Eq. (8)):

$$2Al^{3+} + 3HS^- + 3OH^- \rightarrow Al_2S_3 + 3H_2O. \tag{8}$$

Table 6 Name of a few compounds present in significant quantities in neem leaf extract identified from GC-MS analysis

Time (min)	Name of the compound	Area (%)	Compound group
53.08	18-Norcholest-17(20),24-dien-21-oic acid, 16-acetoxy-4,8,14-trimethyl-3,11-dioxo, methyl ester	27.58	Ester
49.7	(5'β)Spiro(1,3-dithiane)-2,2'-(androstan-3'-ol), 17'-acetoxy-3'β-methyl-	14.17	Heterocyclic sulfur compound
50.25	Cholest-5-ene-16,22-dione, 3β,26-dihydroxy-, 3-acetate, (20S,25R)-	17.12	Ester
50.8	psi.,.psi.-Carotene, 1,1',2,2'-tetrahydro-1,1'-dimethoxy	16.96	Tetraterpene
23.6	Neophytadiene	1.19	Diterpene
27.7	Lactose	8.46	Disaccharide
30.6	Phytol	2.19	Diterpene alcohol
38.0	Hexadecanoic acid, 2-hydroxy-1-(hydroxymethyl)ethyl ester	2.04	Ester
48.4	Stigmasterol	3.98	Sterol
14.5	Melezitose	2.01	Trisaccharide
43.42	3-[3-Bromophenyl]-7-chloro-3,4-dihydro-10-hydroxy-1,9(2H,10H)-acridinedion	0.54	Heterocyclic nitrogen

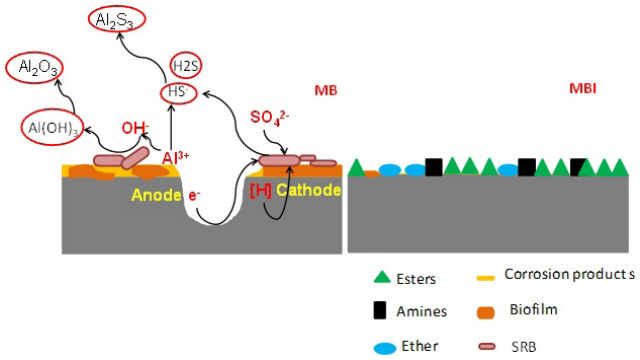

Fig. 13 Mechanism involved in the biocorrosion of Al3102 with and without NLE

Aluminium ions also react with hydroxyl ions to form $Al(OH)_3$ which further forms Al_2O_3 (Eq. (9)):

$$Al(OH)_3 \rightarrow 0.5Al_2O_3 + 1.5H_2O. \quad (9)$$

The Al_2S_3 formed dissolve in the corrosive medium to give raise to the formation of $Al(OH)_3$ (Eq. (10)):

$$0.5Al_2S_3 + 3H_2O \rightarrow Al(OH)_3 + 1.5H_2S. \quad (10)$$

In the presence of neem leaf extract, the cathodic reaction rate is highly affected as observed from the potentiodynamic polarization results. The metabolic activity of *DD* is decreased which can be justified by the absence of sulfide in the MBI sample in the XPS studies. The SEM analysis also shows no biofilm formation in the MBI sample. However, the corrosive effects of the medium have caused a little corrosion which causes Al_2O_3 and $Al(OH)_3$ to form. Adsorbed compounds from NLE offer protection against the chemical effects of corrosion which can be verified from the presence of many functional groups representing compounds that have been identified in the NLE.

4 Conclusions

The effect of *Desulfovibrio desulfuricans* on Al3102 was investigated in modified Baar's medium. Though a thicker biofilm formed on the exterior of Al3102, the occurrence of *DD* caused severe pitting corrosion on the alloy. The *DD* attack caused a five to ten times increase in the C_R of Al3102 with reference to the control. SEM analysis showed significant pitting corrosion and more sessile bacteria on the alloy's surface. The addition of 1000 ppm of NLE effectively controls the *DD*-influenced corrosion. The average inhibition efficiency of 82% and 80% were observed in the weight loss and PDP studies, respectively. Electrochemical investigations reveal that the effectiveness of the inhibitor lasts for two weeks and decreases slightly for the third and fourth weeks. Investigations using XPS and EDAX confirm the adsorption of NLE molecules on the sample. Corrosion products composed of Al_2S_3, $Al(OH)_3$ and Al_2O_3.

References

[1] Victoria, S. N., Sharma, A., Manivannan, R. "Metal corrosion induced by microbial activity – Mechanism and control options", Journal of the Indian Chemical Society, 98(6), 100083, 2021. https://doi.org/10.1016/j.jics.2021.100083

[2] Woldman, N. E., Frick, J. "Woldman's Engineering Alloys", ASM International, 2000. ISBN 0871706911

[3] de Andrade, J. S., Vieira, M. R. S., Oliveira, S. H., de Melo Santos, S. K., Urtiga Filho, S. L. "Study of microbiologically induced corrosion of 5052 aluminum alloy by sulfate-reducing bacteria in seawater", Material Chemistry and Physics, 241, 122296, 2020. https://doi.org/10.1016/j.matchemphys.2019.122296

[4] Guan, F., Zhai, X., Duan, J., Zhang, J., Li, K., Hou, B. "Influence of sulfate-reducing bacteria on the corrosion behavior of 5052 aluminum alloy", Surface and Coatings Technology, 316, pp. 171–179, 2017. https://doi.org/10.1016/j.surfcoat.2017.02.057

[5] Guan, F., Duan, J., Zhai, X., Wang, N., Zhang, J., Lu, D., Hou, B. "Interaction between sulfate-reducing bacteria and aluminum alloys—Corrosion mechanisms of 5052 and Al-Zn-In-Cd aluminum alloys", Journal of Materials Science & Technology, 36, pp. 55–64, 2020. https://doi.org/10.1016/j.jmst.2019.07.009

[6] Cai, H., Peng, W., Chen, X., Wang, Y., Zhang, D. "Sulfide ions-induced release of biocides from a metal-phenolic supramolecular film fabricated on aluminum for inhibition of microbially influenced corrosion", Corrosion Science, 167, 108534, 2020. https://doi.org/10.1016/j.corsci.2020.108534

[7] Wang, P., Lu, Z., Zhang, D. "Slippery liquid-infused porous surfaces fabricated on aluminum as a barrier to corrosion induced by sulfate reducing bacteria", Corrosion Science, 93, pp. 159–166, 2015. https://doi.org/10.1016/j.corsci.2015.01.015

[8] Lam, H., Oh, D.-C., Cava, F., Takacs, C. N., Clardy, J., De Pedro, M. A., Waldor, M. K. "D-amino acids govern stationary phase cell wall remodeling in bacteria", Science, 325(5947), pp. 1552–1555, 2009. https://doi.org/10.1126/science.1178123

[9] Swaroop, B. S., Victoria, S. N., Manivannan, R. "*Azadirachta indica* leaves extract as inhibitor for microbial corrosion of copper by *Arthrobacter sulfureus* in neutral pH conditions—A remedy to blue green water problem", Journal of the Taiwan Institute of Chemical Engineers, 64, pp. 269–278, 2016. https://doi.org/10.1016/j.jtice.2016.04.007

[10] Sharma, A., Manivannan, R., Victoria, S. N. "Investigation of SRB induced biocorrosion of mild steel and its control", Journal of the Indian Chemical Society, 97, pp. 1029–1032, 2020. [online] Available at: http://indianchemicalsociety.com/portal/uploads/journal/July-13.PDF [Accessed:15 March 2023]

[11] Song, Z., Cai, H., Liu, Q., Jiang, L., Chu, H. "Performance of corrosion inhibitor extracted from enzymatic hydrolysate of waste Platanus acerifolia leaves", Journal of Industrial and Engineering Chemistry, 111, pp. 464–479, 2022. https://doi.org/10.1016/j.jiec.2022.04.027

[12] Fu, W. "Investigation of type II of microbiologically influenced corrosion (MIC) mechanism and mitigation of MIC using novel green biocide cocktails", MSc Thesis, The Russ College of Engineering and Technology of Ohio University, 2013.

[13] Ametek Scientific Instruments "ZSimpWin software", [computer program] Available at: https://www.ameteksi.com/products/software/zsimpwin [Accessed: 15 March 2022]

[14] Lv, M., Du, M., Li, X., Yue, Y., Chen, X. "Mechanism of microbiologically influenced corrosion of X65 steel in seawater containing sulfate-reducing bacteria and iron-oxidizing bacteria", Journal of Materials Research and Technology, 8(5), pp. 4066–4078, 2019. https://doi.org/10.1016/j.jmrt.2019.07.016

[15] Cogger, N. D., Evans, N. J. "An introduction to electrochemical impedance measurement", Solartron Limited, Hampshire, UK, Rep. 6, 1999.

[16] Meeusen, M., Visser, P., Macía, L. F., Hubin, A., Terryn, H., Mol, J. M. C. "The use of odd random phase electrochemical impedance spectroscopy to study lithium-based corrosion inhibition by active protective coatings", Electrochimica Acta, 278, pp. 363–373, 2018. https://doi.org/10.1016/j.electacta.2018.05.036

[17] Mittal, K. L. "Silanes and other coupling agents", CRC Press, 2007. ISBN 9789067644525

[18] Prakashaiah, B. G., Kumara, D. V., Pandith, A. A., Shetty, A. N., Rani, B. E. A. "Corrosion inhibition of 2024-T3 aluminum alloy in 3.5% NaCl by thiosemicarbazone derivatives", Corrosion Science, 136, pp. 326–338, 2018. https://doi.org/10.1016/j.corsci.2018.03.021

[19] Szubert, K., Wojciechowski, J., Majchrzycki, Ł., Jurczak, W., Lota, G., Maciejewski, H. "The rapeseed oil based organofunctional silane for stainless steel protective coatings", Materials, 13(10), 2212, 2020. https://doi.org/10.3390/ma13102212

[20] Fonseca, I. T. E., Feio, M. J., Lino, A. R., Reis, M. A., Rainha, V. L. "The influence of the media on the corrosion of mild steel by Desulfovibrio desulfuricans bacteria: an electrochemical study", Electrochimica Acta, 43(1–2), pp. 213–222, 1998. https://doi.org/10.1016/S0013-4686(97)00227-2

[21] Hong, T., Jepson, W. P. "Corrosion inhibitor studies in large flow loop at high temperature and high pressure", Corrosion Science, 43(10), pp. 1839–1849, 2001. https://doi.org/10.1016/S0010-938X(01)00002-6

[22] Wu, Y., Lin, Y., Xu, J. "Synthesis of Ag–Ho, Ag–Sm, Ag–Zn, Ag–Cu, Ag–Cs, Ag–Zr, Ag–Er, Ag–Y and Ag–Co metal organic nanoparticles for UV-Vis-NIR wide-range bio-tissue imaging", Photochemical & Photobiological Sciences, 18(5), pp. 1081–1091, 2019. https://doi.org/10.1039/C8PP00493E

[23] Lodowska, J., Wolny, D., Jaworska-Kik, M., Kurkiewicz, S., Dzierżewicz, Z., Węglarz, L. "The chemical composition of endotoxin isolated from intestinal strain of *Desulfovibrio desulfuricans*", The Scientific World Journal, 2012, 647352, 2012. https://doi.org/10.1100/2012/647352

[24] Śliwak, A., Grzyb, B., Díez, N., Gryglewicz, G. "Nitrogen-doped reduced graphene oxide as electrode material for high rate supercapacitors", Applied Surface Science, 399, pp. 265–271, 2017. https://doi.org/10.1016/j.apsusc.2016.12.060

[25] Yoshida, N., Totsuka, M., Ino, J., Matsumoto, S. "Surface passivation of $In_{0.52}Al_{0.48}As$ using $(NH_4)_2S_x$ and $P_2S_5/(NH_4)_2S$", Japanese Journal of Applied Physics, 33, 1248, 1994. https://doi.org/10.1143/JJAP.33.1248

[26] McGuire, G. E., Schweitzer, G. K., Carlson, T. A. "Study of core electron binding energies in some group IIIa, Vb, and VIb compounds", Inorganic Chemistry, 12(10), pp. 2450–2453, 1973. https://doi.org/10.1021/ic50128a045

[27] van der Laan, G., Westra, C., Haas, C., Sawatzky, G. A. "Satellite structure in photoelectron and Auger spectra of copper dihalides", Physical Review B, 23(9), pp. 4369–4380, 1981. https://doi.org/10.1103/PhysRevB.23.4369

[28] Liu, H., Huang, L., Huang, Z., Zheng, J. "Specification of sulfate reducing bacteria biofilms accumulation effects on corrosion initiation", Materials and Corrosion, 58(1), pp. 44–48, 2007. https://doi.org/10.1002/maco.200603984

[29] Paulo, C., Kenney, J. P. L., Persson, P., Dittrich, M. "Effects of phosphorus in growth media on biomineralization and cell surface properties of marine Cyanobacteria *Synechococcus*", Geosciences, 8(12), 471, 2018. https://doi.org/10.3390/geosciences8120471

[30] Chen, S., Wang, P., Zhang, D. "Corrosion behavior of copper under biofilm of sulfate-reducing bacteria", Corrosion Science, 87, pp. 407–415, 2014. https://doi.org/10.1016/j.corsci.2014.07.001

[31] Chavan, P. P., Sapner, V. S., Sathe, B. R. "Enhanced electrochemical NO^{2-} oxidation reactions on biomolecule functionalised graphene oxide", Chemistry Select, 6(24), pp. 6050–6055, 2021. https://doi.org/10.1002/slct.202100608

[32] Dec, W., Mosiałek, M., Socha, R. P., Jaworska-Kik, M., Simka, W., Michalska, J. "Characterization of *Desulfovibrio desulfuricans* biofilm on high-alloyed stainless steel: XPS and electrochemical studies", Materials Chemistry and Physics, 195, pp. 28–39, 2017. https://doi.org/10.1016/j.matchemphys.2017.04.011

[33] Kaur, R., Tiwari, A., Manish, M., Maurya, I. K., Bhatnagar, R., Singh, S. "Common garlic (*Allium sativum* L.) has potent Anti-*Bacillus anthracis* activity", Journal of Ethnopharmacology, 264, 113230, 2021. https://doi.org/10.1016/j.jep.2020.113230

[34] Yang, X., Shao, J., Liu, Z., Zhang, D., Cui, L., Du, C., Li, X. "Stress-assisted microbiologically influenced corrosion mechanism of 2205 duplex stainless steel caused by sulfate-reducing bacteria", Corrosion Science, 173, 108746, 2020. https://doi.org/10.1016/j.corsci.2020.108746